

# Distortion-Dependent Raman Spectra and Mode Mixing in $RMnO_3$ Perovskites

M. N. Iliev<sup>1</sup>, M. V. Abrashev<sup>2</sup>, J. Laverdière<sup>3</sup>, S. Jandl<sup>3</sup>, M. M. Gospodinov<sup>4</sup>, Y.-Q. Wang<sup>1</sup>, and Y.-Y. Sun<sup>1</sup>

<sup>1</sup>Texas Center for Superconductivity and Department of Physics, University of Houston, Texas 77204-5002, USA

<sup>2</sup>Faculty of Physics, University of Sofia, 1164 Sofia, Bulgaria

<sup>3</sup>Département de Physique, Université de Sherbrooke, Sherbrooke, Canada J1K 2R1 and

<sup>4</sup>Institute of Solid State Physics, Bulgarian Academy of Sciences, 1184 Sofia, Bulgaria

(Dated: August 10, 2018)

The polarized Raman spectra of orthorhombic  $RMnO_3$  series ( $R=La,Pr,Nd,Sm,Eu,Gd,Tb,Dy,Ho,Y$ ) were studied at room temperature. The variation of phonon frequencies with  $R$  ionic radius  $r_R$  as a whole confirms the commonly accepted Raman line assignments with two noticeable exceptions: (1) with decreasing  $r_R$  the stretching  $A_g(1)$  and bending  $A_g(3)$  modes strongly mix for  $R=Sm$  to  $Tb$ , while for further decrease or  $r_R$  ( $R=Dy,Ho,Y$ ) the  $A_g(3)$  mode is observed at higher frequency than  $A_g(1)$  mode; (2) similar distortion-dependent mode mixing takes place for the rotational  $A_g(2)$  and  $O1(x)$  [ $A_g(7)$ ] modes. The mode mixing is particularly strong for the  $RMnO_3$  compounds with  $r_R$  values close to the transition from A-type to incommensurate sinusoidal antiferromagnetic ordering at low temperatures. The frequency of rotational  $A_g(2)$  and  $A_g(4)$  modes scales to the angles of  $MnO_6$  [101] and [010] rotations, respectively, and could be used as a measure of their value.

PACS numbers: 78.30.-j, 63.20.Dj, 75.47.Lx

## I. INTRODUCTION

Until recently the  $RMnO_3$  perovskites ( $R=rare\ earth,Y,Sc$ ) have been object of research mainly as parent materials of mixed valence manganites exhibiting colossal magnetoresistivity (CMR).[1, 2, 3, 4] In the past few years, however, there is an increased interest in the complex relationships among the lattice distortions, magnetism, dielectric and transport properties of undoped  $RMnO_3$ . [5, 6, 7, 8, 9, 10] In particular, it has been found that with decreasing radius ( $r_R$ ) of  $R$  ( $R=La$  to  $Eu$ ) the transition temperature  $T_N$  to A-type antiferromagnetic (A-AFM) structure also decreases. With further decrease of  $r_R$  ( $R=Gd$  to  $Ho$ ) the magnetic structure below  $T_N$  changes from A-AFM to incommensurate antiferromagnetic one(IC-AFM) with sine-wave ordering of the Mn moments with temperature-dependent wave vector  $\vec{k}_s = (k_s, 0, 0)$  along the  $a$ -axis (in  $Pnma$  notations). At  $T_{lock} < T_N$  an incommensurate-to-commensurate (IC-CM) transition takes place and  $k_s$  locks at a value  $< 0.4$ . [8] A transition to commensurate E-type antiferromagnetic structure (E-AFM,  $k_s = 0.5$ ) has been observed below  $T_{lock} = 26K$  only for  $HoMnO_3$ . [6] For  $TbMnO_3$  and  $DyMnO_3$  it was found that the IC-CM transition is accompanied by a ferroelectric transition, associated with lattice modulation in the CM phase.[7, 9]. Large magnetodielectric effects have also been reported for orthorhombic  $HoMnO_3$ , and  $YMnO_3$ . [11]

Although the role of lattice distortions in the interplay of magnetic, dielectric and transport properties of  $RMnO_3$  perovskites is widely recognized, there are relatively few studies on the variations of these distortions with  $R$ . [10, 12] Raman spectroscopy can provide significant additional information on the distortions and their variations with both  $R$  and temperature. The Raman active modes in  $RMnO_3$  ( $7A_g + 5B_{1g} + 7B_{2g} + 5B_{3g}$ )

are activated exclusively due to the deviations from ideal perovskite structure and in principle the activation of each Raman line can with definite certainty be assigned to the value of one or two types of basic distortion (rotations of  $MnO_6$  octahedra around [101] or [010] directions, Jahn-Teller distortion, or shift of  $R$  atoms).[13] The first assignment of the Raman lines in the spectra of  $RMnO_3$  to definite atomic vibrations has been done by comparison of experimentally obtained Raman phonon frequencies of  $LaMnO_3$  and  $YMnO_3$  with those predicted by lattice dynamical calculations (LDC). [14] Although for most of the experimentally observed Raman lines the frequencies have been in good agreement with those predicted by LDC, some uncertainties about the phonon line assignment remained. Indeed, some Raman lines of same symmetry have close frequencies and due to the approximations of the LDC model one reasonably expects some difference between measured and calculated values. The assignment of the two  $A_g$  Raman lines between 450 and 520  $cm^{-1}$ , where are the  $A_g$  modes corresponding to anti-stretching(AS) and bendings(B) of  $MnO_6$  octahedra, has been challenged by Martin-Carron et al.[15] in a Raman study of several  $RMnO_3$  perovskites ( $R=La,Pr,Nd,Tb,Ho,Er,Y$ ). Based on the fact that the Mn-O distances exhibit only small changes within the  $RMnO_3$  series, they assigned the AS band observed near 480-490  $cm^{-1}$  to the anti-stretching mode, while the B band which shifts from  $\approx 450$   $cm^{-1}$  in  $LaMnO_3$  to  $\approx 530$   $cm^{-1}$  in  $ErMnO_3$  has been assigned to bending mode(s). An obvious problem of this re-assignment is the "crossing" of the AS and B modes, which are of the same  $A_g$  symmetry.

In this work we present results of a detailed study of polarized Raman spectra of  $RMnO_3$  ( $R=La,Pr,Nd,Sm,Eu,Gd,Tb,Dy,Ho,Y$ ) at room temperature. The comparison of variations with  $R$  of phonon

frequencies and relative intensities of most pronounced  $A_g$  and  $B_{2g}$  modes shows that some corrections of previous phonon mode assignment are needed. The strong mixing and spectral weight transfer between  $A_g$  anti-stretching (AS) and bending (B) modes in the  $500\text{ cm}^{-1}$  region, most clearly observed for  $R=\text{Eu,Gd}$  and Tb, correlates with changes of magnetic structure. Similar distortion-dependent mode mixing is observed for the rotational  $A_g(2)$  and  $O1(x)$  [ $A_g(7)$ ] modes.

## II. SAMPLES AND EXPERIMENTAL

$\text{PrMnO}_3$ ,  $\text{NdMnO}_3$  and  $\text{SmMnO}_3$  samples were grown by the floating zone method described in Ref.[16]. Single crystals of  $\text{DyMnO}_3$  of average sizes  $1 \times 1 \times 2\text{ mm}^3$  were prepared following a procedure to be described elsewhere [17]. Orthorhombic  $\text{YMnO}_3$ ,  $\text{HoMnO}_3$  samples were prepared under pressure as described in Ref.[11]. For  $R=\text{Eu,Gd,Tb}$  the precursor powders were heated at  $1130\text{-}1160^\circ\text{C}$  in  $\text{O}_2$  for 24 hours. Although the samples (except for  $\text{DyMnO}_3$ ) were polycrystalline, the size of the constituting microcrystals was larger than the laser spot. It was possible to select microcrystals with crystallographic orientation such that the spectra in parallel and crossed scattering configurations were dominated by  $A_g$  or  $B_{2g}$  contributions, respectively. For exact separation of the  $A_g$  and  $B_{2g}$  spectra the SPECTRA SUBTRACT program of the GRAMS AI software package was used.

The Raman spectra were measured at room temperature in backscattering configuration using two different spectrometers: Labram-800 and Jobin Yvon HR640, both equipped with microscope and liquid-nitrogen-cooled CCD detector. The spectra obtained with  $514.5\text{ nm}$  ( $\text{Ar}^+$ ) and  $632.8\text{ nm}$  ( $\text{He-Ne}$ ) were practically identical.

## III. RESULTS AND DISCUSSION

The  $A_g$  and  $B_{2g}$  spectra of  $\text{RMnO}_3$  as obtained at room temperature are shown in Figure 1. With same scattering configuration the absolute value of Raman intensities were increasing with decreasing R ionic radius ( $r_R$ ). For better comparison the  $A_g$  and  $B_{2g}$  spectra were normalized to the integrated intensities of  $A_g(1) + A_g(3)$  and  $B_{2g}(1)$  lines, respectively. At least five  $A_g$  and four  $B_{2g}$  lines are clearly pronounced and the variations of their parameters with  $R$  can be followed with a good accuracy. The phonon line frequencies are given in Table I.

The correlation between structural and physical parameters of  $\text{RMnO}_3$  perovskites may be described as a function of different parameters, such as the ionic radius  $r_R$ , tolerance factor  $t$  or the averaged tilt angle  $\Psi$ . The relation between these parameters, however, is close to linear[10] and any one of them can be used for characterization of phonon mode frequency variations. Figure 2 shows the dependence of Raman phonon frequencies

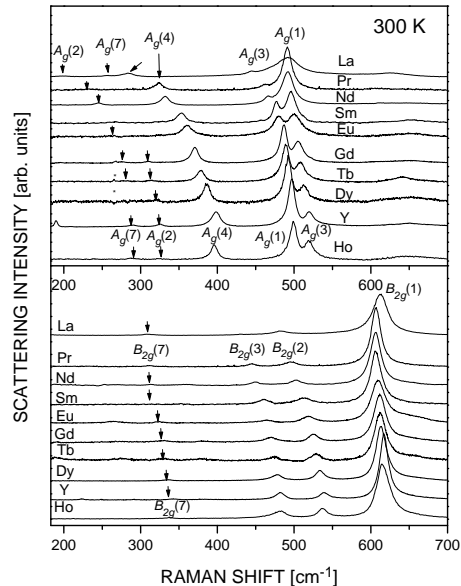


FIG. 1:  $A_g$  and  $B_{2g}$  Raman spectra of  $\text{RMnO}_3$  at room temperature. The phonon mode notations correspond to those of Refs.[13, 14]. The  $A_g$  and  $B_{2g}$  spectra are normalized to the integrated intensity of  $A_g(1) + A_g(3)$  and  $B_{2g}(1)$  lines, respectively.

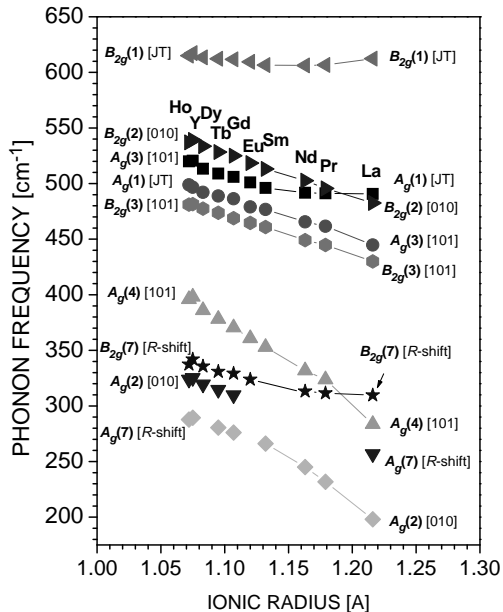


FIG. 2: Variations of phonon mode frequencies with  $R$  ionic radius  $r_R$ .

TABLE I: Frequencies (in  $\text{cm}^{-1}$ ) of the experimentally observed  $A_g$  and  $B_{2g}$  Raman lines of  $RMnO_3$  at room temperature.

Mode	Main atomic motions	La	Pr	Nd	Sm	Eu	Gd	Tb	Dy	Ho	Y	Basic distortion
$A_g(1) \rightarrow A_g(3)$	O2 anti-stretching $\rightarrow$ MnO <sub>6</sub> bending	490.7	491.2	491.7	496.1	501.0	506.0	509.0	513.4	520.0	520.6	JT,[010] $\rightarrow$ [101]
$A_g(3) \rightarrow A_g(1)$	MnO <sub>6</sub> bending $\rightarrow$ O2 anti-stretching	444.8	461.8	465.6	476.7	479.0	486.4	488.8	492.1	498.9	496.7	[101] $\rightarrow$ JT,[010]
$A_g(4)$	out-of-phase MnO <sub>6</sub> $x$ -rotations	283.6	323.7	331.8	352.9	360.8	370.5	378.2	386.0	395.9	398.1	[101]
$A_g(2) \rightarrow A_g(7)$	in-phase MnO <sub>6</sub> $y$ -rotations $\rightarrow$ O1( $x$ )	256.8					309.8	314.6	319.5	323.8	325.3	[010] $\rightarrow$ $R$ -shift
$A_g(7) \rightarrow A_g(2)$	O1( $x$ ) $\rightarrow$ in-phase MnO <sub>6</sub> $y$ -rotations	198.1	231.8	245.0	266.1		276.1	280.5		287.8	289.4	$R$ -shift $\rightarrow$ [010]
$B_{2g}(1)$	in-plane O2 stretching	612.3	606.7	606.2	606.6	609.5	611.7	612.2	613.5	615.0	617.3	JT
$B_{2g}(2)$	in-phase O2 "scissors'-like	482.5	495.7	502.6	513.1	518.4	525.0	528.4	533.6	537.0	539.2	[010]
$B_{2g}(3)$	out-of-phase MnO <sub>6</sub> bending	430.0	444.8	449.1	460.9	464.6	468.9	473.7	477.5	481.1	481.5	[101]
$B_{2g}(7)$	O1( $z$ )	309.7	311.5	313.2		323.8	329.2	330.9	335.6		342.0	$R$ -shift

on  $r_R$ . Most Raman frequencies  $\omega_i$  exhibit nearly linear increase with  $r_R$ , but the slope  $\Delta\omega_i/\Delta r_R$  depends mainly on the type of the mode (stretching, bending or rotational) as well on the type of distortion that has activated the corresponding mode in the Raman spectrum (MnO<sub>6</sub> rotations around [010]<sub>c</sub> or [101]<sub>c</sub> cubic axes, Jahn-Teller(JT) distortion, and  $R$ -shift).[13]

### A. Basic distortions and Raman modes in $RMnO_3$

In the ideal cubic ABO<sub>3</sub> perovskite (space group  $Pm\bar{3}m$ ,  $Z = 1$ ) all atoms are at centrosymmetrical sites with fixed coordinates and there are no Raman allowed modes. The structure of stoichiometric  $RMnO_3$ , described at room temperature by the  $Pnma$  space group ( $Z = 4$ ), can be considered as orthorhombically distorted superstructure of the ideal perovskite with [100]<sub>o</sub>, [010]<sub>o</sub>, and [001]<sub>o</sub> directions coinciding with the [101]<sub>c</sub>, [010]<sub>c</sub> and [101]<sub>c</sub> directions of the parent cubic structure. In the  $Pnma$  structure the atoms occupy four non-equivalent atomic sites ( $R, Mn, O1, O2$ ), of them only the Mn site is a center of symmetry. From symmetry considerations only 5 of the 12 atomic coordinates are fixed [ $R$ -1, Mn-3, O1-1], while the remaining 7 variable coordinates can be considered as the lattice degrees of freedom producing the above mentioned lattice distortion. These distortions give rise to 24 ( $7A_g + 5B_{1g} + 7B_{2g} + 5B_{3g}$ ) Raman-allowed phonon modes, which in turn can be assigned to their distortions of origin ([010]-, [101]-rotation, JT, or  $R$ -shift). With decreasing  $r_R$  the distortions increase and most of the bond lengths shorten, which reasonably results in twofold effect: enhanced Raman intensity and hardening of Raman frequencies.

At first sight the [010] and [101] rotations can directly be obtained from the O2-Mn-O2 and O1-Mn-O1 angles, which practically have equal values.[10, 12] As shown by Abrashev et al.[13], however, even in the case of equal O-Mn-O angles, the [010] and [101] rotation angles will be different. They are related to the deviations ( $x_i, y_i, z_i$ ,  $i$ -atomic index) of  $Pnma$  atomic coordinates from those in a hypothetical undistorted perovskite structure as

$$\Psi_{[010]} = \arctan(2|x_{O2} - z_{O2}|)$$

$$\Psi_{[101]} = \arctan(2^{5/2}|y_{O2}|) \approx \arctan(2^{3/2}|z_{O1}|)$$

The so defined atomic deviations can also be used to describe the other two basic distortions, namely, the JT distortion, characterized by the relative difference  $D_{JT} = |\Delta d_{Mn-O2}| / \langle d_{Mn-O2} \rangle$  of the two pairs of Mn-O2 distances, and the shift  $D_R(x)$  of the  $R$ -atoms in  $x$ -direction from their positions in an undistorted perovskite. In the case of small distortions:

$$D_{JT} = 2|x_{O2} + z_{O2}|$$

$$D_{R(x)} = 2x_R$$

The variations of the basic distortions, calculated using the available data for atomic positions in  $RMnO_3$ [10, 12] are given in Table II.

### B. Pure and mixed stretching (Jahn-Teller) modes

The frequency of a mode involving mainly stretching vibrations of O2 atoms in the  $xz$  planes is determined by the Mn-O2 distances. The short and long Mn-O2 bond lengths vary with  $r_R$  within 0.5% and 1.1%, respectively[10, 12] and therefore one expects that  $\omega_{stretch} \propto d_{Mn-O2}^{3/2}$  will change by no more than 1.5%. As illustrated in Figure 3, this is exactly the case for the  $B_{2g}(1)$  mode at 606-617  $\text{cm}^{-1}$ , which has been assigned to the in-phase O2 stretching.[14]. The minimum of  $B_{2g}(1)$  frequency near  $R=Nd, Sm$  reflects the fact that for these  $R$ 's the averaged Mn-O distance has a maximum.

Based on the same bond-length considerations, one could expect that the Raman line of  $A_g$  symmetry at 490-495  $\text{cm}^{-1}$ , corresponding to the in-phase anti-stretching vibrations of O2 in the  $xz$  plane,[14] would behave in a similar way and its frequency would remain nearly constant through the whole  $RMnO_3$  series. As seen from Fig.4, this is obviously not the case. The data of Figs. 1 and 4 clearly show a classic example for mixing of modes of same symmetries and close frequencies. For large  $r_R$  ( $R=La, Pr, Nd$ ) the lines at 490-492 and 445-465  $\text{cm}^{-1}$  can be considered as pure stretching( $A_g(1)$ )

TABLE II: Variations with  $R$  of the four basic distortions of the  $Pnma$  structure. The data for  $\text{SmMnO}_3$  and  $\text{GdMnO}_3$  have been obtained by the fit of corresponding experimental data for rest  $R\text{MnO}_3$  compounds.[10, 12]

Distortion	Measure	La	Pr	Nd	Sm	Eu	Gd	Tb	Dy	Ho	Y
[010]	$\Psi_{[010]}$ [deg]	9.23	11.43	12.11	13.07	13.35	13.60	13.81	14.00	14.16	14.11
[101]	$\Psi_{[101]}$ [deg]	12.17	13.53	14.08	15.10	15.49	15.86	16.24	16.59	16.90	16.82
JT	$ \Delta d_{Mn-O2}  / \langle d_{Mn-O2} \rangle$	0.0647	0.0665	0.0652	0.0612	0.0597	0.0582	0.0574	0.0571	0.0575	0.0573
$R$ -shift	$2x_R$	0.097	0.129	0.138	0.151	0.155	0.159	0.166	0.167	0.169	0.168
$\langle \text{Mn-O2} \rangle$ Refs.[10]	Å	2.044	2.063	2.067		2.066			2.065		
$\langle \text{Mn-O2} \rangle$ Refs.[12]	Å	2.043	2.059	2.062				2.063	2.063	2.064	2.052

and bending ( $A_g(3)$ ) modes, respectively. With decreasing  $r_R$  the  $A_g(3)$  frequency increases and approaches that of  $A_g(1)$ , resulting in strong mode mixing evidenced by mode repulsion and transfer of intensity. The mixing is most strongly pronounced for  $R=\text{Sm}$  to  $\text{Tb}$  where the two modes are of comparable intensities and involve both stretching and bending atomic motions. With further decrease of  $r_R$  ( $R=\text{Dy}, \text{Ho}, \text{Y}$ ) the modes become less mixed but now the higher mode is dominated by  $\text{MnO}_6$  bending [ $A_g(3)$ -type] motions and the lower one is  $A_g(1)$ -type.

Two phonon modes of same symmetries and close frequencies can be considered as coupled quantum oscillators. In a good approximation their frequencies are given by

$$\omega_{1,2} = \frac{\omega' + \omega''}{2} \pm \sqrt{\frac{(\omega' - \omega'')^2}{4} + \frac{V^2}{4}}$$

where  $\omega'$  and  $\omega''$  are the mode frequencies without coupling and  $V$  is the coupling constant. It is reasonable to assume that without coupling the  $A_g(1)$  and  $A_g(3)$  mode frequencies would depend on  $r_R$  in the same way as the  $B_{2g}(1)$  and  $B_{3g}(3)$  modes, respectively, as both modes of the  $A_g(1)$ - $B_{2g}(1)$  (stretching) and  $A_g(3)$ - $B_{2g}(3)$  (bending) pairs are activated by the same basic distortion and have similar shape. Therefore, as shown with dash lines in Fig.4, the  $\omega'(r_R)$  dependence for the uncoupled  $A_g(1)$  mode can be approximated by scaling the experimental  $B_{2g}$  values, whereas that of uncoupled  $A_g(3)$  mode [ $\omega''(r_R)$ ], like in the case of  $B_{2g}(3)$ , can be approximated by a linear dependence. At the crossing point ( $r_R \approx 1.125$  Å),  $\omega'(1.125) = \omega''(1.125)$ , which gives  $V = \omega_1(1.125) - \omega_2(1.125) \approx 20$   $\text{cm}^{-1}$ .

### C. Pure and mixed rotational ("soft") modes

The frequency vs  $\Psi_{[101]}$  dependence for the  $A_g(4)$  mode involving mainly  $\text{MnO}_6$   $x$ -rotations, shown in Fig.4 with full circles, is close to proportionality. Expectedly, this mode exhibits "soft mode" behavior with  $\omega(\Psi) \rightarrow 0$  for  $\Psi \rightarrow 0$ , the slope of  $\omega^{A_g(4)}(\Psi_{[101]})$  being 23.5  $\text{cm}^{-1}/\text{deg}$ . Calculations of lattice dynamics for the two end compounds  $\text{LaMnO}_3$  and  $\text{YMnO}_3$  have shown that the two weak  $A_g$  modes at lower frequencies are strongly mixed and involve both in-phase  $\text{MnO}_6$   $y$ -rotations [ $A_g(2)$ ] and  $\text{O1}(x)$ -motions [ $A_g(7)$ ]. The higher

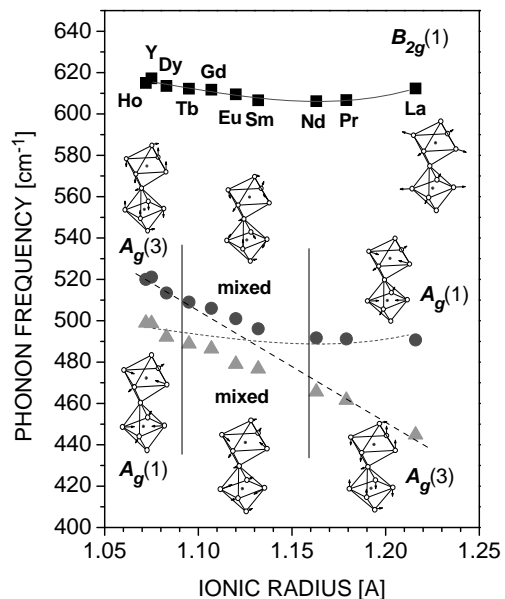


FIG. 3: Variations with  $r_R$  of the frequencies of  $B_{2g}(1)$ ,  $A_g(3)$  and  $A_g(1)$  modes. The dashed curves show the expected  $\omega'(r_R)$  and  $\omega''(r_R)$  dependences for pure stretching and bending modes.

of these modes is  $A_g(7)$ -like in  $\text{LaMnO}_3$ , but  $A_g(2)$ -like in  $\text{YMnO}_3$ . Assuming that the higher mode remains  $A_g(2)$ -like in other compounds with small  $r_R$  ( $\text{HoMnO}_3$ ,  $\text{DyMnO}_3$ ,  $\text{TbMnO}_3$ ,  $\text{GdMnO}_3$ ), one finds that the frequency vs  $\Psi_{[010]}$  dependence for the partly mixed  $A_g(2)$  mode (shown with empty squares) is practically the same as that for the pure  $A_g(4)$  mode. Interestingly, the frequencies of [111]-rotational modes of structurally different rhombohedral  $\text{LaMnO}_3$  and  $\text{LaAlO}_3$  fit to these dependences, which is an indication for a quite general relationship between the angle of rotation and frequency of the rotational "soft" modes in perovskitelike compounds, independent on the direction of the rotational axis.

### D. $R$ -shift modes

The weak  $A_g(7)$  and  $B_{2g}(7)$  involve mainly  $\text{O1}$  motions in the  $xz$  plane, activated in the Raman spectrum due to the shift of  $R^{3+}$  ions from their positions in an ideal

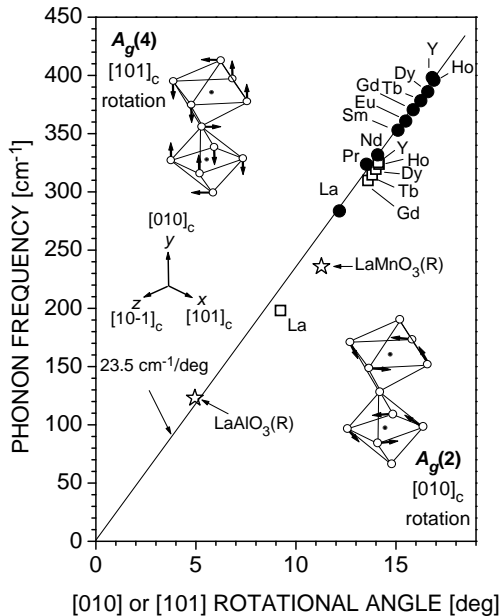


FIG. 4: Variations with the tilt angle  $\Psi_{[101]}$  or  $\Psi_{[010]}$  of the frequencies of  $A_g(4)$  and  $A_g(2)$  modes, involving mainly  $MnO_6$  rotations.

perovskite. It follows from Fig.2, Table I and Table II that in the case of pure  $R$ -shift mode [ $B_{2g}(7)$ ], despite of strongly increasing  $R$ -shift distortion between  $R=La$  and  $Y$ , the corresponding increase of mode frequency is

relatively modest (see Table II). It is plausible to expect similar dependence on  $r_R$  for the  $A_g(7)$  mode, which explains the above discussed observation that the frequency vs  $r_R$  dependence of the mixed  $A_g(2) + A_g(7)$  modes is governed mainly by their rotational [ $A_g(2)$ ] component.

#### IV. CONCLUSION

The comparative study of polarized Raman spectra of orthorhombic  $RMnO_3$  series ( $R=La, Pr, Nd, Sm, Eu, Gd, Tb, Dy, Ho, Y$ ) shows that the variations of lattice distortions with  $r_R$  affect significantly both the phonon frequencies and the shape of some Raman phonon modes. The strong mixing of phonon modes involving in-plane and out-of-plane oxygen motions may become a clue for understanding the change with  $r_R$  of magnetic ordering at low temperatures. The established proportionality between the frequency of a rotational mode and the angle of corresponding rotational distortion may be used for material characterization.

#### Acknowledgments

This work is supported in part by the State of Texas through the Texas Center for Superconductivity and the National Science and Engineering Research Council of Canada. The work of M.M.G. is supported by the Bulgarian National Research Fund (Project F-1207).

- 
- [1] R.M. Kusters, J. Singleton, D.A. Keen, R. McGreevy, and W. Hayes, *Physica B* **155**, 362 (1989).
  - [2] R. von Helmolt, J. Wecker, B. Holzappel, L. Schultz, and K. Samwer, *Phys. Rev. Lett.* **71**, 2331 (1993).
  - [3] S. Jin, T. H. Tiefel, M. McCormack, R. A. Fastnacht, R. Ramesh, and L. H. Chen, *Science* **64**, 413 (1994).
  - [4] Y. Tokura, A. Urushibara, Y. Moritomo, T. Arima, A. Asamitsu, G. Kido, and N. Furukawa, *Science* **63**, 3931 (1994).
  - [5] A. Munoz, M. T. Casáis, J. A. Alonso, M. J. Martínez-Lope, J. L. Martínez, and M. T. Fernández-Díaz, *Inorg. Chem.* **40**, 1020 (2001).
  - [6] A. Munoz, J. A. Alonso, M. T. Casais, M. J. Martínez-Lope, J. L. Martínez, and M. T. Fernández-Díaz, *J. Phys.: Condens. Matter* **14**, 3285 (2002).
  - [7] T. Kimura, T. Goto, H. Shintani, K. Ishizaka, T. Arima, and Y. Tokura, *Nature* **426**, 55 (2003).
  - [8] T. Kimura, S. Ishihara, H. Shintani, T. Arima, K. T. Takahashi, K. Ishizaka, and Y. Tokura, *Phys. Rev. B* **68**, 060403(R) (2003).
  - [9] T. Goto, T. Kimura, G. Lawes, A. P. Ramirez, and Y. Tokura, *Phys. Rev. Lett.* **92**, 257201 (2004).
  - [10] B. Dabrowski, S. Kolesnik, A. Baszczuk, O. Chmaissem, T. Maxwell, and J. Mais, *J. Solid State Chem.* **178**, 629 (2005).
  - [11] B. Lorenz, Y. Q. Wang, Y. Y. Sun, and C. W. Chu, *Phys. Rev. B* **70**, 212412 (2004).
  - [12] J. A. Alonso, M. J. Martínez-Lope, M. T. Casais, and M. T. Fernández-Díaz, *Inorg. Chem* **39**, 917 (2000).
  - [13] M. V. Abrashev, J. Bäckström, L. Börjesson, V. N. Popov, R. A. Chakalov, N. Kolev, R.-L. Meng, and M. N. Iliev, *Phys. Rev. B* **65**, 184301 (2002).
  - [14] M. N. Iliev, M. V. Abrashev, H. G. Lee, V. N. Popov, Y. Y. Sun, C. Thomsen, R. L. Meng, and C. W. Chu, *Phys. Rev. B* **57**, 2872 (1998).
  - [15] L. Martín-Carrón, A. de Andrés, M. J. Martínez-Lope, M. T. Casais, and J. A. Alonso, *Phys. Rev. B* **66**, 174303 (2002).
  - [16] A. M. Balbashov, S. G. Karabashev, Y. A. M. Mukovskii, and S. A. Zverkov, *J. Cryst. Growth* **167**, 365 (1996).
  - [17] M. M. Gospodinov et al, unpublished results.